Comparative analysis of mediastinal fat-associated lymphoid cluster development and lung cellular infiltration in murine autoimmune disease models and the corresponding normal control strains

Short title: Mediastinal lymphoid clusters in murine autoimmune disease models

Yaser Hosny Ali Elewa[1,2], Osamu Ichii[2], Yasuhiro Kon[2,*]

[1]Department of Histology and Cytology, Faculty of Veterinary Medicine, Zagazig University, Zagazig 44519, Egypt

[2]Laboratory of Anatomy, Department of Biomedical Sciences, Graduate School of Veterinary Medicine, Hokkaido University, Sapporo 060-0818, Japan

***Corresponding author**: Yasuhiro Kon, DVM, PhD, Laboratory of Anatomy, Department of Biomedical Sciences, Graduate School of Veterinary Medicine, Hokkaido University, Kita 18, Nishi 9, Kita-ku, Sapporo 060-0818, Japan.

Email: y-kon@vetmed.hokudai.ac.jp.

Tel: 008011-706-5187

Fax: 008011-706-5189

Key words: autoimmune disease model, lymphoid cluster, mediastinal adipose tissue

Abbreviations: HE, hematoxylin and eosin; LCs, lymphoid clusters; LTi, lymphoid tissue inducer; MFALCs, mediastinal fat-associated lymphoid clusters; MFT, mediastinal fat tissue; NK, natural killer; RA, rheumatoid arthritis; SLE, systemic lupus erythematosus

Summary

We previously discovered mediastinal fat-associated lymphoid clusters (MFALCs) as novel lymphoid clusters (LCs) associated with mediastinal fat tissue (MFT) in healthy mice. However, no data about their morphology in immune-associated disease conditions, and their relationship with lung infiltration, is available to date. In the present study, we compared the morphological features of MFALCs in 4-month-old male murine autoimmune disease models (MRL/MpJ-*lpr* mice and BXSB/MpJ-*Yaa* mice) with those of the corresponding control strains (MRL/MpJ and BXSB/MpJ, respectively). In addition, we analyzed their correlation with lung infiltration. Furthermore, immunohistochemistry for CD3, B220, Iba1, Gr1, and BrdU was performed to detect T- and B-cells, macrophages, granulocytes, and proliferating cells, respectively. The spleen/body weight ratios and anti-dsDNA autoantibody titers were found to be significantly higher in the autoimmune models than in the control strains. Furthermore, the autoimmune model presented prominent MFALCs, with a significantly greater ratio of LC area to total MFT area, and more apparent diffused cellular infiltration into the lung lobes than the other studied strains. Higher numbers of T- and B-cells, macrophages, and proliferating cells, but fewer granulocytes, were observed in the autoimmune models than in the control strains. Interestingly, a significant positive Pearson's correlation between the size of the MFALCs and the density of CD3-, B220-, and Iba1-positive cells in the lung was observed. Therefore, our data suggest a potentially important role for MFALCs in the progression of lung disease. However, further investigation is required to clarify the pathological role of MFALCs in lung disease, especially in inflammatory disorders.

INTRODUCTION

The immune response against microbes and toxins involves cooperation between both innate and adaptive immunity [1]. The innate immune system, which mounts an immediate response against infection, thereby constituting the first line of defense [2], is also required for the activation of the adaptive immune response via antigen presentation. There are two types of adaptive immune responses: humoral immunity, which is mediated by antibody-producing B-cells, and cell-mediated immunity, mediated by T-cells. The lymphocytes of the innate immune system do not express antigen receptors, as observed in T- and B-cells; however, these lymphocytes produce cytokines and rapidly exert cytotoxic activity against virus-infected cells [3,4]. The innate lymphocytes include classical natural killer (NK) and lymphoid tissue inducer (LTi) cells, in addition to the recently reported T helper 2 (Th2)-type innate lymphocytes, such as natural helper (NH) cells [5]. NH cells were first discovered in novel lymphoid structures associated with mesenteric adipose tissue in both humans and mice [6]. These lymphoid structures are referred to as mesenteric fat-associated lymphoid clusters (FALCs). Recently, we found similar lymphoid clusters associated with mediastinal adipose tissue in mice, and referred to these as mediastinal FALCs (MFALCs) [7].

Our previous study revealed strain-related differences in MFALCs among three strains of healthy mice: Th1-biased C57BL/6N, Th2-biased DBA/2Cr, and autoimmune-prone MRL/MpJ mice. We revealed that C57BL/6N mice presented a significantly larger number and size of MFALCs compared with DBA/2Cr and MRL/MpJ strains [7]. Interestingly, Th1-biased C57BL/6 mice are susceptible to hypersensitive pneumonitis, a granulomatous inflammatory lung disease caused by repeated inhalation of organic antigens in humans and mice [8,9]; however, Th2-biased DBA/2 mice are resistant [10,11]. This suggests that the development of MFALCs may affect intrapleural immune conditions. However, there have been no data suggesting an association between MFALCs and intrapleural organs such as the lung.

In humans, systemic lupus erythematosus (SLE) may affect numerous organs, including

intrapleural organs [12]. The most common thoracic manifestation of SLE is pleuritis [13]. Pleuritis occurs in 17–60% of patients at some point during the course of SLE [14]. Although severe parenchymal lung disease is uncommon, pulmonary complications of SLE include acute lupus pneumonitis, diaphragmatic dysfunction and shrinking lung syndrome, cavitating pulmonary nodules, pulmonary hypertension, pulmonary vasculitis, pulmonary embolism (often due to circulating anticardiolipin antibodies), alveolar hemorrhage (reflecting diffuse endothelial injury), and chronic interstitial pneumonitis [15-18].

Murine SLE models also exhibit thoracic manifestations [19]. The MRL/MpJ-*lpr* mouse model carries the lymphoproliferation (*lpr*) mutation in the apoptosis-related *Fas* gene, resulting in autoreactive lymphocyte proliferation. This mouse model, which closely mimics SLE in humans, exhibits lymphadenopathy, splenomegaly, hypergammaglobulinemia with anti-double strand DNA (dsDNA) antibodies leading to tissue deposition and injury in various organs, including the lung and kidney [20-22]. These pathophysiological processes are mediated by immune complex deposition, complement activation, and infiltration of inflammatory leukocytes [23,24]. The BXSB/MpJ-*Yaa* model also develops systemic autoimmune disease at around 5–7 months of age, and males show more severe autoimmune symptoms than females due to the Y-linked autoimmune acceleration (*Yaa*) mutation on the Y chromosome [25-27]. Autoimmune disease phenotypes of this strain were characterized by the presence of autoantibodies, hypergammaglobulinemia, splenomegaly, glomerulonephritis, and dacryoadenitis [28]. However, the pathological features of intrapleural organs in SLE remain unclear.

In the present study, we demonstrate that MFALCs are significantly larger in size in autoimmune disease model mice than in the corresponding control strains. Additionally, we show that the size of these MFALCs is positively correlated with immune cell infiltration into the lung tissue. This is the first report of the development of MFALCs in autoimmune disease model mice, and of the pathological correlation between MFALCs and inflammatory processes in the lung. These

data emphasize the crucial roles of MFALCs in immunological functions in the intrathoracic environment.

MATERIALS AND METHODS

Experimental animals

Autoimmune disease model mice (MRL/MpJ-*lpr* and BXSB/MpJ-*Yaa*) and healthy control mice (MRL/MpJ, and BXSB/MpJ) were utilized in the present study. Mice were purchased from Japan SLC, Inc., (Shizuoka, Japan) (n = 5/strain) and examined at 4 months of age. In handling the experimental animals, the investigators adhered to the Guide for the Care and Use of Laboratory Animals, Hokkaido University, Graduate School of Veterinary Medicine (approved by the Association for Assessment and Accreditation of Laboratory Animal Care International).

Tissue preparation and microscopy

Following euthanasia by deep anesthesia, blood was collected from the carotid arteries and the mediastinal fat tissue (MFT), the lungs, and spleens were removed and fixed with 4% paraformaldehyde. In order to preserve lung architecture, the lungs were inflated with 4% paraformaldehyde prior to immersion in fixative solution. After overnight fixation, specimens were dehydrated in graded alcohol and embedded in paraffin. Subsequently, 3-µm-thick paraffin sections of MFTs were deparaffinized, rehydrated, stained with hematoxylin and eosin (HE), and observed under a light microscope.

Immunohistochemistry

Immunohistochemical analysis for B220, CD3, Gr1 (Ly-6G), and Iba1 was performed using 3-µm-thick paraffin sections to detect B-cells, pan-T-cells, granulocytes, and macrophages, respectively. Immunohistochemical procedures were performed according to our previous report [29]. In order to detect cell proliferation, BrdU+ cells were observed within the MFALCs and lungs of the strains studied. The detection of BrdU+ cells was performed according to our previous report [7]. The details of the antigen retrieval method used, as well as of the sources and dilutions of

antibodies used are listed in Table 1. Sections of the spleen were used as positive controls and stained simultaneously with the MFTs and lung lobes (cranial right, middle right, caudal right, accessory right lobes, and left lobe) using the abovementioned antibodies. The sections representing negative controls were incubated in 0.01 M phosphate buffered saline without primary antibody (data not shown).

ELISA for serum autoantibody

Serum levels of anti-dsDNA autoantibodies were determined by ELISA using dsDNA-coated plates purchased from Alpha Diagnostic Intl. Inc (M-5110; San Antonio, TX, USA). The assay was performed according to the manufacturer's instructions

Histoplanimetry

For histoplanimetry, 5 mice were analyzed per strain. The spleen weights and spleen/body weight ratios were compared between the different mouse strains. For measurement of the lymphoid cluster (LC) area / the total MFT area ratio, light micrographs of HE-stained MFT sections from each strain were prepared. The areas of LCs and the total areas of the mediastinal white adipose tissue within the MFT were measured using ImageJ software (ver. 1.32j, http://rsb.info.nih.gov/ij) and the lymphoid cluster (LC) area / the total MFT area ratio was calculated as reported previously [7].

Based on the immunohistochemistry staining images, the percentages of B220-, CD3-, Gr1-, and Iba1-positive cells in MFALCs were calculated in 3 different sections from each mouse. These were presented as the positive cell index for each cell population by counting the number of immunopositive cells and dividing them by the total number of mononuclear cells within the MFALCs. In addition, the densities of immunopositive cells / unit area (0.094 mm^2) in different lung

168 lobes were compared between the different strains.

169

170 *Statistical analysis*

171 All numerical results are presented as the means ± standard error (SE). The results for the
172 different groups were compared using analysis of variance (ANOVA). We used the nonparametric
173 Mann-Whitney *U* test for comparison between the autoimmune disease mouse models and the
174 normal control strains ($P < 0.05$). The correlation between the density of CD3-, B220-, Gr1-, and
175 Iba1-positive cells in different lung lobes, and the percentage of lymphoid cluster areas in the total
176 MFT areas, in the mouse strains was analyzed by Pearson's correlation test (*significant value, $P <$
177 0.05, **highly significant value, $P < 0.01$).

178

Results

Autoimmune disease onset

Spleen weights and spleen/body weight ratios were found to be significantly higher in the autoimmune mouse models (MRL/MpJ-*lpr* and BXSB/MpJ-*Yaa*) than in the controls (MRL/MpJ, and BXSB/MpJ) (Fig. 1a and b respectively). The spleen weights of the MRL/MpJ-*lpr* and BXSB/MpJ-*Yaa* mice were almost 3.2-fold and 3.3-fold higher than those of the MRL/MpJ and BXSB/MpJ mice, respectively. Moreover, the spleen/body weight ratios of the MRL/MpJ-*lpr* and BXSB/MpJ-*Yaa* mice were almost 2.8-fold and 3.1-fold higher than those of the MRL/MpJ and BXSB/MpJ mice, respectively. With respect to serum anti-dsDNA antibody levels, a significantly higher titer was observed in MRL/MpJ-*lpr* and BXSB/MpJ-*Yaa* mice than in MRL/MpJ and BXSB/MpJ mice (Fig. 1c).

Morphological features of MFALCs

Analysis of the HE-stained sections indicated that MFALCs were observed in the white adipose tissue of the MFTs, in all mice examined, with varying sizes among the studied strains (Fig. 2). The size of the MFALCs was more prominent in the autoimmune models, MRL/MpJ-*lpr* and BXSB/MpJ-*Yaa* (Figs. 2b and d) than in the MRL/MpJ, and BXSB/MpJ mice (Figs. 2a and c). With respect to the histological index of MFALCs development (as expressed by the ratio of the LC area to the total MFT area), a significantly higher LC/MFT area ratio was observed in the autoimmune disease models than in the control strains (Fig. 2e).

MFALC immune cell populations

In order to assess the population of immune cells in the MFALCs, immunohistochemical analysis for CD3, B220, Iba1, and Gr1 was performed to detect pan-T-cells, B-cells, macrophages, and granulocytes, respectively. CD3-, B220-, and Iba1-positive cells (Figs. 3a-c) were found to

predominate in all strains examined, with the presence of a few Gr1-positive cells (Fig. 3d).

In order to assess the immune cell populations in MFALCs, the percentages of immunopositive cells in the total cells detected in MFALCs were analyzed in the different mouse strains and represented as cell indices (Fig. 3e). A significant difference was observed between the cell indices of CD3-, B220-, and Iba1-populations in the autoimmune disease models and the corresponding control strains (Figs. 3e). No significant difference was observed between the strains in terms of the percentage of Gr1-positive cells (data not shown).

Proliferating cells in the MFALCs

BrdU-positive cells, whose numbers varied by strain, were observed in the MFALCs (Fig. 4). A greater number of BrdU-positive cells was observed within the MFALCs of the autoimmune disease model mice (Fig. 4b and d) than in the MFALCs of the control strains (Fig. 4a and c). In particular, the number of BrdU-positive cells in the MFALCs of MRL/MpJ-*lpr* mice was greater than in those of the other strains studied (Fig. 4b).

Histopathological features of the lungs

Analysis of the HE-stained sections indicated that MRL/MpJ (Figs. 5a and b) mice showed normal histological lung architecture, characterized by normal blood vessels, thin interalveolar septum, and a low degree of cell infiltration. However, the lungs in MRL/MpJ-*lpr* and BXSB/MpJ-*Yaa* mice, as well as BXSB/MpJ mice, showed several histopathological alterations characterized by the presence of numerous congested blood vessels, high numbers of extravasated red blood cells, large accumulations of mononuclear cells, thicker interalveolar septa, and numerous abnormal and collapsed alveoli (Figs. 5c-h).

Immune cell infiltration in the lung lobes

Immunohistochemical analysis revealed the infiltration of CD3-, B220-, Iba1-, and Gr1-positive cells in the mouse lungs (Figs. 6a-d). Mononuclear cells positive for CD3-, B220-, and Gr1 were mainly observed in the interalveolar septum and interstitium (Figs. 6a, b, and d). Iba1-positive cells were mainly observed in the connective tissues of the peribronchial regions as well as in the lung dust cells (Fig. 6d).

Within the same strain, no significant difference was observed in the density of immunopositive cells in the left and right (cranial, middle, caudal, and accessory) lobes (data not shown). However, a significant difference was observed in the density of CD3-, B220-, and Iba1-positive cell infiltration between the lungs of autoimmune disease model mice (MRL/MpJ-*lpr* and BXSB/MpJ-*Yaa* mice) and those of the control strains (Fig. 6e). There was a significant difference in the density of Gr1-positive cell infiltration between MRL/MpJ-*lpr* mice and the corresponding normal control strain; however, no significant difference was observed between the lung of BXSB/MpJ-*Yaa* mice and its counterpart control strain (Fig. 6e).

Correlation between the MFLAC development, autoimmune disease indices, and cellular infiltration of the lungs

Significant positive correlation was observed between the autoimmune disease model mice (MRL/MpJ-*lpr* and BXSB/MpJ-*Yaa*) and the control strains in terms of the size of the MFALCs and the spleen weights, spleen/body weight ratios, and serum anti-dsDNA antibody levels (Table 2). The size of the MFALCs was also significantly positively correlated with the density of CD3-, B220- and Iba1-positive cell infiltration in the lung lobes (Table 3). Positive correlation was also observed between the size of MFALCs and the density of Gr-1 positive cell infiltration in the lung lobes (Table 3). The later correlations were found to be significant between the BXSB/MpJ-*Yaa* mice and corresponding controls ($r = 0.733^{*}$). However, no significant correlation was observed between MRL/MpJ-*lpr* and the counterpart control strain ($r = 0.077$).

Discussion

In previous studies, we demonstrated the presence of LCs associated with MFT, similar to those discovered in the mesenteric adipose tissue of both humans and mice [6], in apparently normal mice strains. These were termed MFALCs [7]. In addition, we showed that there are significant differences in MFALC size in normal mice, and determined that the predominant cells in MFALCs were lymphocytes [7]. However, there have been no data on the morphology of such MFALCs in autoimmune disease model mice. We reported an association between the LCs and mediastinal white adipose tissue. In addition, we found that the autoimmune disease models (MRL/MpJ-*lpr* and BXSB/MpJ-*Yaa*) exhibit better developed MFALCs than the control strains. White adipose tissue, which secretes adipokines such as leptin, adiponectin, visfatin, and resistin, is considered the largest endocrine organ. These adipokines function as hormones in glucose homeostasis and appetite regulation, and as cytokines in the immune system, where they mediate effects on autoimmunity [30,31,32,33]. In addition, they have been reported to play roles in autoimmune rheumatic diseases, such as SLE and rheumatoid arthritis [33].

In the present study, the autoimmune disease models, MRL/MpJ-*lpr* and BXSB/MpJ-*Yaa*, were reported to develop SLE-like disorders characterized by lymphoid activation and hyperplasia, nephritis, splenomegaly, and elevated serum autoantibodies against dsDNA [20,34]. MRL/MpJ-*lpr* and BXSB/MpJ-*Yaa* mice presenting MFALCs of larger size also exhibited higher spleen weights and spleen/body weight ratios as well as higher serum anti-dsDNA autoantibody levels than the normal control strains. Numerous mononuclear cells within the MFALCs of the autoimmune disease model mice showed bromodeoxyuridine-incorporating activity, suggesting local cell proliferation [7]. Therefore, we suggest that the presence of prominent lymphoproliferation in the MFTs of the autoimmune model mice examined may represent an SLE-like phenotype in addition to other previously reported phenotypes.

It has been reported that pulmonary involvement may be an important contributor to morbidity

279 and mortality in human SLE [15,35,36]. The MRL/MpJ-*lpr* mouse model has been used to study the
280 progress of pulmonary inflammation in SLE [37]. Perivascular lymphocytic infiltration in the lung
281 has been reported to precede renal involvement in such murine models of lupus [38]. Lung disorders
282 secondary to SLE include interstitial pneumonitis with mononuclear cellular infiltration, interstitial
283 fibrosis, edema, and pulmonary vasculitis [35]. Accordingly, our findings revealed a greater
284 accumulation of mononuclear cells with histopathological changes such as numerous congested
285 blood vessels, thicker interalveolar septa, and several abnormal and collapsed alveoli in the lungs of
286 MRL/MpJ-*lpr* and BXSB/MpJ-*Yaa* mice as well as in BXSB/MpJ mice than in the other strains
287 studied. The interstitial mononuclear infiltration in the lung lobes observed in these strains may
288 reflect the inflammatory processes associated with interstitial pneumonitis in human SLE [15,36].
289 CD3-positive T cells, B220-positive B cells, Iba1-positive macrophages, and Gr-1-positive
290 granulocytes were observed in both MFALCs and the lung. Interestingly, the autoimmune disease
291 models showed significantly higher numbers of CD3-, B220-, and Iba1- positive cells, in both the
292 MFALCs and the lung, than the control strains. Furthermore, both the MFALCs and lungs in
293 MRL/MpJ-*lpr* mice showed a higher number of CD3-positive cells than those of the other strains.
294 Massive T-cell proliferation was also reported in the spleen and mesenteric lymph node of
295 MRL/MpJ-*lpr* mice compared with C57BL/6 mice [38]. Furthermore, it has been reported that the
296 majority of proliferating lymphoid cells in the lymph nodes of MRL/MpJ-*lpr* mice are T-cells rather
297 than B-cells [39]. Such lymphoproliferation was reported to be due to a massive accumulation of
298 double-negative ($CD3^+$/$CD4^-$/CD8) T-cells in the secondary lymphoid organs [40] resulting from *lpr*
299 mutation of *Fas* [41,42]. On the other hand, the BXSB/MpJ-*Yaa* mice presented a higher number of
300 B220-positive cells, in both MFALCs and lungs, than the other strains studied. Furthermore, we
301 previously reported that BXSB/MpJ-*Yaa* mice develop dacryoadenitis with T- and B-cell infiltration,
302 and demonstrated that B-cells were the predominant infiltrating cells in the lacrimal glands of these
303 mice [28]. Moreover, in BXSB/MpJ-*Yaa* mice, B-cells with the *Yaa* mutation are intrinsically biased

304 towards nucleolar antigens due to increased expression of Toll-like receptors in duplicated regions of
305 the Y chromosome [43]. Therefore, the increased cell infiltration of the lungs would reflect the
306 autoimmune disease conditions in MRL/MpJ-*lpr* and BXSB/MpJ-*Yaa* mice due to the mutation of
307 immune-associated genes (*lpr* mutation of *Fas* in MRL/MpJ-*lpr* mice and mutation in Y
308 chromosome in BXSB/MpJ-*Yaa*). These mutations may characterize the specific immune cell
309 populations of the MFALCs and lungs in each strain.

310 Our data reveal a significantly positive correlation between the size of MFALCs and
311 autoimmune disease indices, including the spleen weights, spleen/ body weight ratios, and serum
312 autoantibody levels, as well as cellular infiltration in the lung, in the autoimmune disease models and
313 control strains. These data clearly indicate a pathological association between MFALCs and
314 autoimmune disease-associated lung pathology. However, differences in the spleen weights and
315 serum autoantibody levels between strains did not fully correspond to differences in MFALC size or
316 density of cellular infiltration in the lung. Briefly, MRL/MpJ mice showed a higher titer of
317 anti-dsDNA antibodies than the other healthy controls, but presented the smallest MFALCs, lowest
318 levels of cellular infiltration in the lung, and lowest spleen weights among the examined strains.
319 Furthermore, although BXSB/MpJ mice presented a relatively higher positive B-cell density in the
320 lung than MRL/MpJ mice, the spleen weights and serum anti-dsDNA antibody levels were
321 comparable to those of the latter strain. These results indicate that the spleen weights and serum
322 anti-dsDNA antibody levels were not directly associated with the development of MFALCs or
323 cellular infiltration in the lung. In addition, the data suggest that not only autoimmune disease
324 phenotypes, but also other factors, are involved in these processes.

325 As reported in our previous study, the MFALCs of Th1-prone C57BL/6 mice were found to
326 be larger in size than those of Th2-prone DBA/2 mice [7]. Furthermore, we recently reported that
327 not only male BXSB/MpJ-*Yaa* mice, but also female BXSB/MpJ mice, clearly exhibit symptoms
328 of age-related autoimmune disease onset, such as increased spleen weights, elevated serum

autoantibodies, and glomerulonephritis, without the contribution of the *Yaa* mutation [44, 45]. For the BXSB/MpJ strain, age-related autoimmune disease onset was attributed to the expression of immune-associated genes in the telomeric regions of chromosome 1 [45]. Therefore, gene mutations as well as genetic backgrounds associated with the immune response may also be important in the development of MFALCs and lung cellular infiltration in murine autoimmune disease models.

In conclusion, our findings indicate a possible role for MFALCs in the development of autoimmune-associated lung diseases. In particular, the elucidation of a positive correlation between the size of MFALCs and density of lung infiltration with mononuclear cells provides insights into the pathogenesis of several intrapleural diseases.

Acknowledgements

This work was supported by the Japan Society for the Promotion of Science, postdoctoral fellowship (JSPS, Number 14F04400). YE designed and performed the experiments, analyzed the data, and wrote the manuscript. OI designed the experiments and wrote the manuscript. YK conceptualized the research, designed the experiments, and wrote the manuscript.

Conflict of Interest

The authors declare no conflict of interest.

References

1. Zygmunt B, Veldhoen M. T helper cell differentiation more than just cytokines. *Adv Immunol* 2011; **109**:159-196.

2. Rasmussen SB, Reinert LS, Paludan SR. Innate recognition of intracellular pathogens: detection and activation of the first line of defense. *APMIS*. 2009; **117**:323-337.

3. Andoniou CE, Andrews DM, Degli-Esposti, MA. Natural killer cells in viral infection: more than just killers. *Immunol Rev* 2006; **214**:239–250.

4. Lodoen MB, Lanier, LL. Natural killer cells as an initial defense against pathogens. *Curr Opin Immunol* 2006; **18**:391–398.

5. Moro K, Yamada T, Tanabe M, Takeuchi T, Ikawa T, Kawamoto H, Furusawa J, Ohtani M, Fujii H, Koyasu S. Innate production of TH2 cytokines by adipose tissue-associated c-Kit^{+} Sca-1^{+} lymphoid cells. *Nature* 2010; **463**:540–544.

6. Koyasu S, Moro K. Innate Th2-type immune responses and the natural helper cell, a newly identified lymphocyte population. *Curr Opin Allergy Clin Immunol* 2011; **11**:109–114.

7. Elewa YH, Ichii O, Otsuka S, Hashimoto Y, Kon Y. Characterization of mouse mediastinal fat-associated lymphoid clusters. *Cell Tissue Res* 2014; **357**:731–741.

8. Fink JN. Hypersensitivity pneumonitis. *Clin Chest Med* 1992; **13**:303–309.

9. Sharma OP, Fujimura N. Hypersensitivity pneumonitis: a noninfectious granulomatosis. *Semin Respir Infect* 1995; **10**:96–106.

10. Gudmundsson G, Monick MM, Gary W. IL-12 modulates expression of hypersensitivity pneumonitis. *J Immunol 1*998; **161:**991–999.

11. Butler NS, Monick MM, Yarovinsky TO, Powers LS, Hunninghake GW. Altered IL-4 mRNA stability correlates with Th1 and Th2 bias and susceptibility to hypersensitivity pneumonitis in two inbred strains of mice. *J Immunol 2*002; **169:**3700–3709.

12. Todd NW, Wise RA. Respiratory complication in the collagen vascular diseases. *Clin Pulm Med* 1996; **3**:101–112.

13. Orens JB, Martinez FJ, Lynch JP III. Pleuropulmonary manifestations of systemic lupus erythematosus. *Rheum Dis Clin North Am* 1994; **20**:159–193.

14. Pandya MR, Agus B, Grady RF. In vivo LE phenomenon in pleural fluid. *Arthritis Rheum* 1976; **19**:962–963.

15. Haupt HM, Moore GW, Hutchins GM. The lung in systemic lupus erythematosus. Analysis of the pathologic changes in 120 patients. *Am J Med* 1981; **71**:791–798.

16. Hedgpeth MT, Boulware DW. Interstitial pneumonitis in antinuclear antibody-negative systemic lupus erythematosus: a new clinical manifestation and possible association with anti-Ro (SS-A) antibodies. *Arthritis Rheum* 1988; **31**:545–548.

17. Weinrib L, Sharma OP, Quismorio FP Jr. A long-term study of interstitial lung disease in systemic lupus erythematosus. *Semin Arthritis Rheum*1990; **20**:48–56.

18. Murin S, Wiedemann HP, Matthay RA. Pulmonary manifestations of systemic lupus erythematosus. *Clin Chest Med* 1998; **19**:641–665.

19. Souza-Fernandes AB, Rocco PR, Contador RS, Menezes SL, Faffe DS, Negri EM, Capelozzi VL, Zin WA. Respiratory changes in a murine model of spontaneous systemic lupus erythematosus. *Respir Physiol Neurobiol* 2006; **153**:107–14.

20. Theofilopoulos AN, Dixon FJ. Murine models of systemic lupus erythematosus. *Adv Immunol* 1985; **37**:269–390.

21. Andrews BS, Eisenberg RA. Theofilopoulos AN. Spontaneous murine lupus-like syndromes. Clinical and immunopathological manifestations in several strains. *J Exper Med* 1978; **148** (5):1198–1215.

22. Reilly CM, Gilkeson GS. Use of genetic knockouts to modulate disease expression in a murine model of lupus, MRL/*lpr* mice. *Immunol Res* 2002; **25**:143–153.

23. Tesch GH, Maifert S, Schwarting A, Rollins BJ, Kelley VR. Monocyte chemoattractant protein 1-dependent leukocytic infiltrates are responsible for autoimmune disease in MRL-Fas (lpr) mice. *J Exp Med* 1999; **190**:1813–1824.

24. Manderson AP, Botto M, Walport MJ. The role of complement in the development of systemic lupus erythematosus. *Annu Rev Immunol* 2004; **22**:431–456.

25. Maibaum MA, Haywood ME, Walport MJ, Morley BJ. Lupus susceptibility loci map within regions of BXSB derived from the SB/Le parental strain. *Immunogenetics* 2000; **51**:370–372.

26. Haywood ME, Rogers NJ, Rose SJ, Boyle J, McDermott A, Rankin JM, Thiruudaian V, Lewis MR, Fossati-Jimack L, Izui S, Walport MJ, Morley BJ. Dissection of BXSB lupus phenotype using mice congenic for chromosome 1 demonstrates that separate intervals direct different aspects of disease. *J Immunol* 2004; **173**:4277–4285.

27. Kimura J, Ichii O, Otsuka S. Kanazawa T, Namiki Y, Hashimoto Y, Kon Y. Quantitative and qualitative urinary cellular patterns correlate with progression of murine glomerulonephritis. *PLoS One* 2011; **6**: e16472.

28. Kosenda K, Ichii O, Otsuka S, Hashimoto Y, Kon Y. BXSB/MpJ-*Yaa* mice develop autoimmune dacryoadenitis with the appearance of inflammatory cell marker messenger RNAs in the lacrimal fluid. *Clin Experiment Ophthalmol* 2013; **41**:788–797.

29. Elewa YH, Bareedy MH, Abuel-Atta AA, Ichii O, Otsuka S, Kanazawa T, Lee S, Hashimoto Y, and Kon Y. Cytoarchitectural differences of myoepithelial cells among goat major salivary glands. *Vet Res Commun* 2010; **34**:557-567.

30. Tilg H, Moschen AR. Adipocytokines: mediators linking adipose tissue, inflammation and immunity. *Nat Rev Immunol* 2006; **6**:772–783.

31. Lago F, Dieguez C, Gomez-Reino J, Gualillo O. The emerging role of adipokines as mediators of inflammation and immune responses. *Cytokine Growth Factor Rev* 2007; **18**:313–325.

32. Guzik TJ, Mangalat D, Korbut R. Adipocytokines‐ novel link between inflammation and vascular function? *J Physiol Pharmacol* 2006; **57**:505–528.

33. Barbosa VS, Rego J, da Silva NA. Possible role of adipokines in systemic lupus erythematosus and rheumatoid arthritis. *Rev Bras Reumatol* 2012; **52**:271–287.

34. Perry D, Sang A, Yin Y, Zheng Y-Y, Morel L. Murine models of systemic lupus erythematosus. *J Biomed Biotechnol* 2011; **2011**:271694.

35. Matthay RA, Schwartz MI, Petty TL, Standord RE, *Gupta RC, Sahn S*A, Steigerwald JC. Pulmonary manifestations of systemic lupus erythematosus: review of twelve cases of acute lupus pneumonitis. *Medicine* 1974; **54:**397–409.

36. Gross M, Esterly JR, Earle RH. Pulmonary alterations in systemic lupus erythematosus. *Am Rev Respir Dis* 1972; **105**:572–577.

37. Sunderrajan EV, McKenzie WN, Lieske TR, Kavanaugh JL, Braun SR, Walker SE. Pulmonary inflammation in autoimmune MRL/Mp-*lpr/lpr* mice. Histopathology and bronchoalveolar lavage evaluation. *Am J Pathol* 1986; **124**:353–362.

38. Theofilopoulos AN, Eisenberg RA, Bourdon M, Crowell JS, Dixon FJ. Distribution of lymphocytes identified by surface markers in murine strain with systemic lupus erythematosus-like syndromes. *J Exp Med* 1979; **149**:516–534.

39. Lewis DE, Grorgi JV, Warner NL: Flow cytometry analysis of T-cells and continuous T-cell lines from autoimmune MRL/I mice. *Nature* 1981; **289**:298–300.

40. Morse H, Davidson W, Yetter R, Murphy E, Roths J, Coffman R. Abnormalities induced by the mutant gene *lpr*: expansion of a unique lymphocytes subset. *J Immunol* 1982; **129**:2612–2615.

41. Suda T, Takahashi T, Golstein P, Nagata S. Molecular cloning and expression of the Fas ligand, a novel member of the tumor necrosis factor family. *Cell* 1993; **75**:1169–1178.

42. Watanabe-Fukunaga R, Brannan C, Copeland N, Jenkins N, Nagata S. Lymphoproliferation disorder in mice explained by defects in Fas antigen that mediates apoptosis. *Nature* 1992; **356**:314–317.

43. Santiago-Raber ML, Kikuchi S, Bore lP, Uematsu S, Akira S, Kotzin BL, Izui S. Evidence for genes in addition to Tlr7 in the *Yaa* translocation linked with acceleration of systemic lupus erythematosus. *J Immunol* 2008; **181**:1556–1562.

44. Merino R, Fossati L, Izui S. The lupus-prone BXSB strain: the *Yaa* gene model of systemic lupus erythematosus. *Springer Semin Immunopathol* 1992; **14**:141–157.

45. Kimura J, Ichii O, Nakamura T, Horino T, Otsuka S, Kon Y. BXSB-type genome causes murine autoimmune glomerulonephritis: pathological correlation between telomeric region of chromosome 1 and *Yaa*. *Genes Immun* 2014; **15**:182–189.

Figure Legends

Figure 1: Indices of autoimmune disease onset in mice

Graph showing the spleen weight (n = 5 mice for each strain) (a), spleen / body weight ratio (n = 5 mice for each strain) (b), and serum anti-double strand DNA (dsDNA) level (n = 4 mice for each strain) (c). Statistically significant difference, as determined using the Mann–Whitney *U*-test ($P < 0.05$), between autoimmune disease models (MRL/MpJ-*lpr* and BXSB/MpJ-*Yaa*) and the control strains (MRL/MpJ, BXSB/MpJ), respectively, is indicated by asterisk (*). Values are shown as the means ± SE.

Figure 2: Histological features of mediastinal fat-associated lymphoid clusters (MFALCs) in mice

Light microscopic images of hematoxylin and eosin (HE)-stained mediastinal fat tissues (MFTs) of MRL/MpJ, MRL/MpJ-lpr, BXSB/MpJ, and BXSB/MpJ-Yaa mice, respectively (a-d). Note that MFALCs (indicated by arrows) are more prominent in both MRL/MpJ-*lpr* (b) and BXSB/MpJ-*Yaa* mice (d). (e) Graph showing the ratio of lymphoid cluster (LC) area to the total MFT area in the HE-stained sections (× 40). Statistically significant difference, as determined using the Mann–Whitney *U*-test ($P < 0.05$); n = 5 mice for each strain, between autoimmune disease models (MRL/MpJ-*lpr* and BXSB/MpJ-*Yaa*) and the control strains (MRL/MpJ, BXSB/MpJ), respectively, is indicated by asterisk (*). Values are shown as the means ± SE.

Figure 3: Immune cells from mediastinal fat-associated lymphoid clusters (MFALCs) in mice

Light microscopic photographs showing immunohistochemical staining of mouse MFALCs with CD3 (a), B220 (b), Iba1 (c), and Gr-1 (d). Numerous CD3-positive T-cells, B220-positive B-cells, and Iba1-positive macrophages (a-c), but only few Gr-1-positive granulocytes (d), are present in mouse MFALCs, and their appearance differs between the strains. Arrows indicate immunopositive cells. Bars (a-d) = 100 μm. Graphs showing the indices of immunopositive cells for CD3 (a), B220

(b), and Iba1 (c) in MRL/MpJ, MRL/MpJ-*lpr*, BXSB/MpJ, and BXSB/MpJ-*Yaa* mice. Statistically significant difference, as determined using the Mann–Whitney *U*-test ($P < 0.05$); n = 5 mice for each strain, between autoimmune disease models (MRL/MpJ-*lpr* and BXSB/MpJ-*Yaa*) and the control strains (MRL/MpJ, BXSB/MpJ), respectively, is indicated by asterisk (*). Values are shown as the means ± SE.

Figure 4: Proliferating cells in the mediastinal fat-associated lymphoid clusters (MFALCs) of the mice

Immunohistochemistry for BrdU in MRL/MpJ (a), MRL/MpJ-*lpr* (b), BXSB/MpJ (c), and BXSB/MpJ-*Yaa* (d) mice. Fewer BrdU-positive cells are visible within the MFALCs of MRL/MpJ and BXSB/MpJ mice (a, c) than in the MFALCs of MRL/MpJ-*lpr* and BXSB/MpJ-*Yaa* mice (b, d) at 4 months.

Figure 5: Histopathological features of the lungs in mice

Light microscopic photographs of hematoxylin and eosin (HE)-stained mouse lung sections of MRL/MpJ (a and b), MRL/MpJ-*lpr* (c and d), BXSB/MpJ (e and f), and BXSB/MpJ-*Yaa* (g and h), mice. The squares in a, c, e, and g indicate the same areas as those in b, d, f, and h, respectively. A greater accumulation of mononuclear cells (asterisks), thicker interalveolar septa (arrows), congested blood vessels (arrowheads), and collapsed alveoli (ca) are visible in the lung tissue of MRL/MpJ-*lpr,* BXSB/MpJ, and BXSB/MpJ-*Yaa* mice (c-h) than in that of MRL/MpJ mice (a and b). Bars = 300 μm (a, c, e, and g). Bars = 50 μm (b, d, f, and h).

Figure 6: Immune cells in the mouse lungs

(a-d) Light microscopic photographs showing immunohistochemical staining of the mouse lungs with CD3 (a), B220 (b), Iba1 (c), and Gr-1 (d). Immunopositive cells (indicated by arrows) are

present in the lungs of MRL/MpJ, MRL/MpJ-*lpr*, BXSB/MpJ, and BXSB/MpJ-*Yaa* mice, and their appearance differs between the strains. In particular, the MRL/MpJ-*lpr* and BXSB/MpJ-*Yaa* mice show a greater abundance of positive cells within the infiltration area. Bars = 50 μm. (a-d) Graph showing the average density of CD3- (a), B220- (b), Iba1- (c), and Gr1- (d) positive cells/unit area in all the lobes in the lungs of MRL/MpJ, MRL/MpJ-*lpr*, BXSB/MpJ, and BXSB/MpJ-*Yaa* mice. Statistically significant difference, as determined using the Mann–Whitney *U*-test ($P < 0.05$); n = 5 mice for each strain, between autoimmune disease models (MRL/MpJ-*lpr* and BXSB/MpJ-*Yaa*) and the control strains (MRL/MpJ, BXSB/MpJ), respectively, is indicated by asterisk (*). Values are shown as the means ± SE.

516 **Table 1**: List of antibodies, working dilutions, and methods for antigen retrieval.

517

Antibody	Source	Dilution	Antigen retrieval	Heating condition
Rabbit anti-CD3	Nichirei (Tokyo, Japan)	1 : 200	Target retrieval solution (high pH) (produced by Dako)	105°C, 20 min
Rat anti-B220	Cedarlane (Ontario, Canada)	1 : 1600	10 mM citrate buffer (pH 6.0)	105°C, 20 min
Rabbit anti-Iba1	Wako (Osaka, Japan)	1 : 1200	10 mM citrate buffer (pH 6.0)	105°C, 20 min
Rat anti-Gr1	R and D system (Minneapolis, USA)	1 : 800	0.1% pepsin/ 0.2 N HCl	37°C, 5 min
Rat anti-BrdU	Abcam (Tokyo, Japan)	1: 200	10 mM citrate buffer (pH 6.0)	105°C, 20 min

518

519 Table 2. Pearson's correlation between the average number of CD3-, B220-, Iba1-, and Gr1-positive
520 cells in all lung lobes and the proportion of lymphoid cluster area in the total MFT areas (expressed
521 as percentages) in autoimmune disease model mice and the normal control strains.

Immune cells		CD3	B220	Iba1	Gr1
MRL/MpJ and	r	0.865**	0.944**	0.656*	0.733*
MRL/MpJ-*lpr*	*P*	0.001	0.000	0.040	0.016
BXSB/MpJ and	r	0.935**	0. 948**	0.762*	0.077
BXSB/MpJ-*Yaa*	*P*	0.000	0.000	0.010	0.832

522 Pearson's correlation test, n = 10, (* Significant, $P < 0.05$; ** Highly significant, $P < 0.01$).

523

524

525 Table 3. Pearson's correlation between spleen weights, spleen/body weight ratios, serum anti-dsDNA
526 antibody level, and the proportion of lymphoid cluster area in total MFT areas (expressed as a
527 percentage) in autoimmune disease model mice and the normal control strains.

Mouse strain		Spleen weight	Spleen/body weight ratios	Serum anti-dsDNA antibody level
MRL/MpJ and	r	0.647*	0.685*	0.816*
MRL/MpJ-*lpr*	*P*	0.043	0. 029	0.013
BXSB/MpJ and	r	0.685*	0.632*	0.745*
BXSB/MpJ-*Yaa*	*P*	0.029	0.050	0.034

528 Pearson's correlation test, n ≥ 8, (*, Significant, P < 0.05; **, Highly significant, P < 0.01).

Figure 1

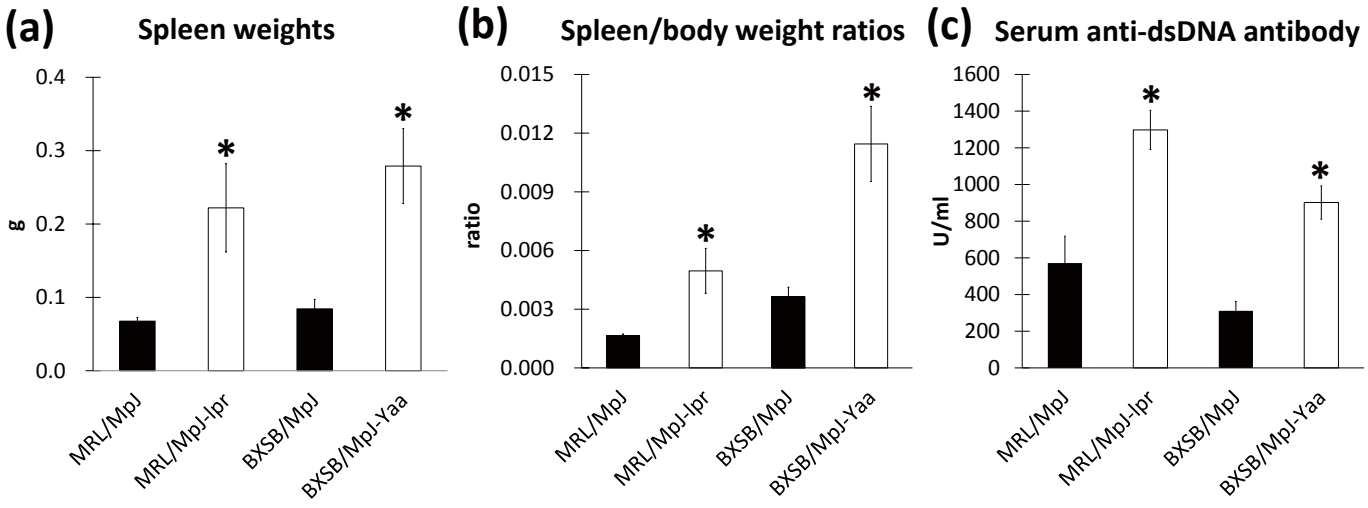
(a)
Spleen weights
g
0.4
0.3
0.2
0.1
0.0
*
*
MRL/MpJ
MRL/MpJ-lpr
BXSB/MpJ
BXSB/MpJ-Yaa
(b)
Spleen/body weight ratios
ratio
0.015
0.012
0.009
0.006
0.003
0.000
*
*
MRL/MpJ
MRL/MpJ-lpr
BXSB/MpJ
BXSB/MpJ-Yaa
(c)
Serum anti-dsDNA antibody
U/ml
1600
1400
1200
1000
800
600
400
200
0
*
*
MRL/MpJ
MRL/MpJ-lpr
BXSB/MpJ
BXSB/MpJ-Yaa

Figure 2

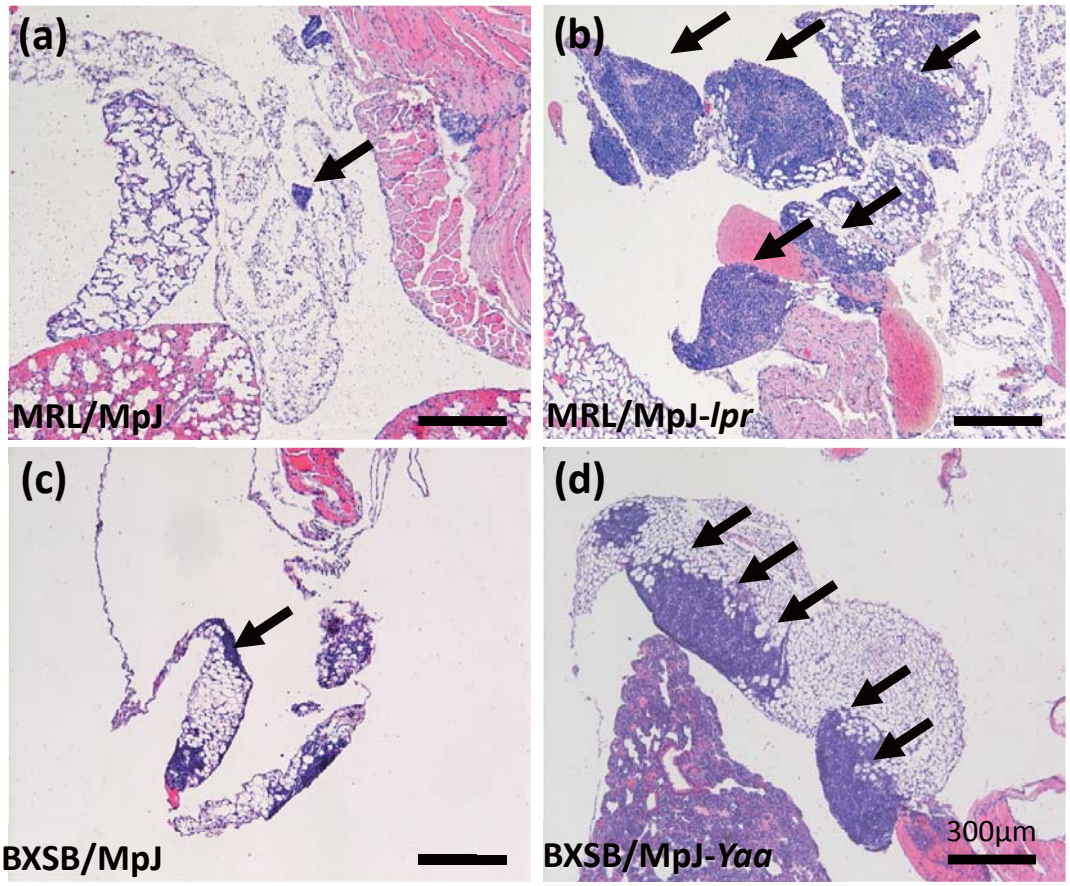
(a)
MRL/MpJ
(b)
MRL/MpJ-*lpr*
(c)
BXSB/MpJ
(d)
BXSB/MpJ-*Yaa*
300μm

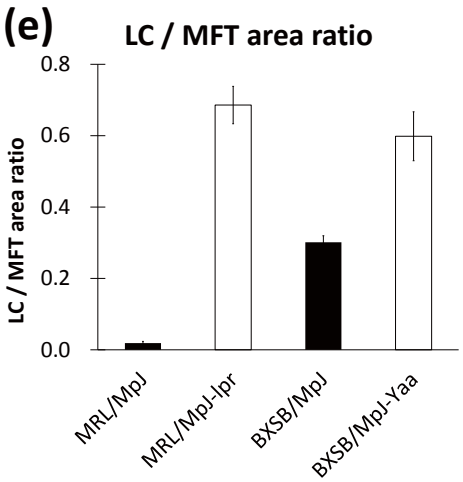
(e)
LC / MFT area ratio
LC / MFT area ratio
0.8
0.6
0.4
0.2
0.0
MRL/MpJ
MRL/MpJ-lpr
BXSB/MpJ
BXSB/MpJ-Yaa

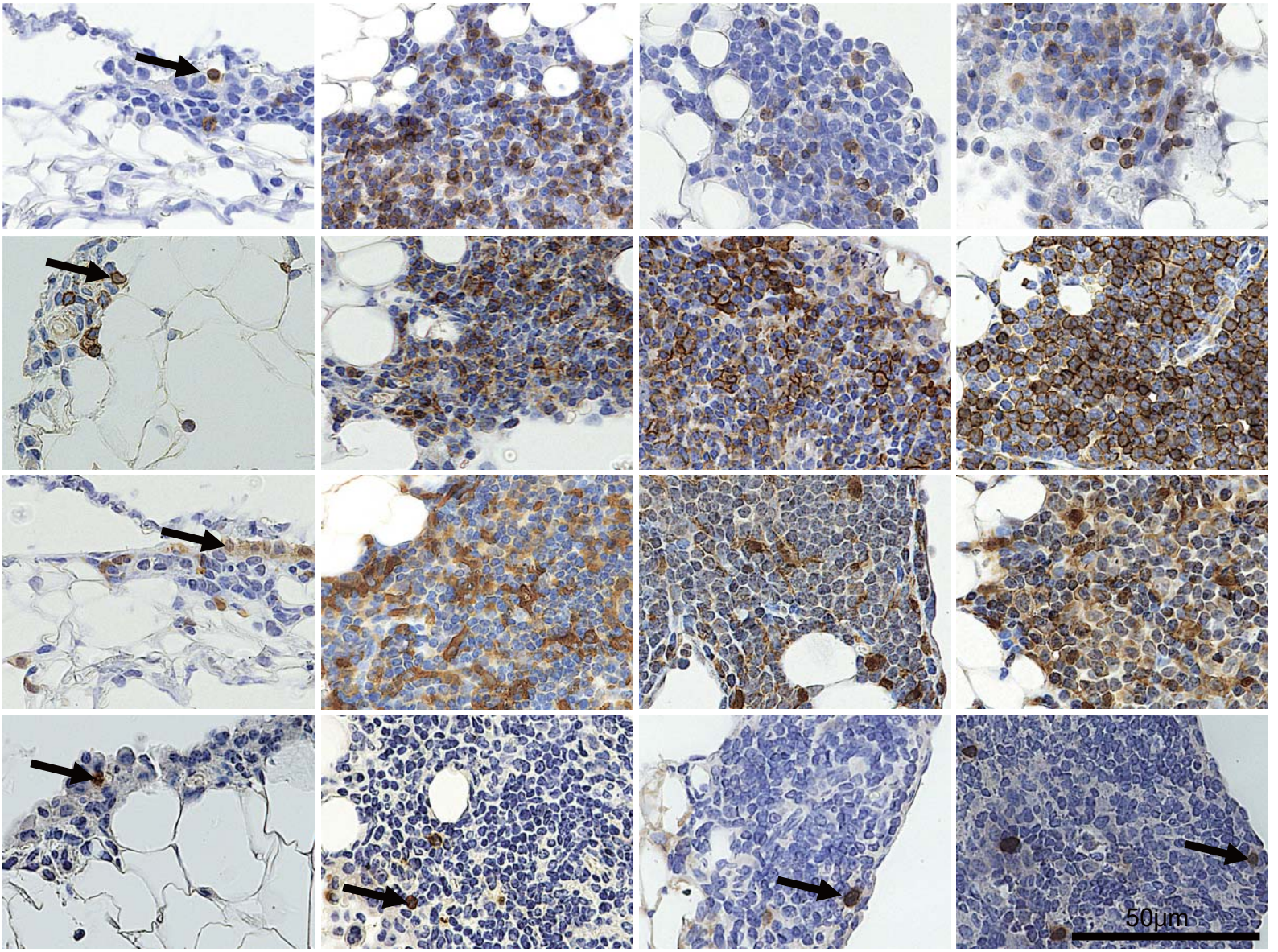
50μm

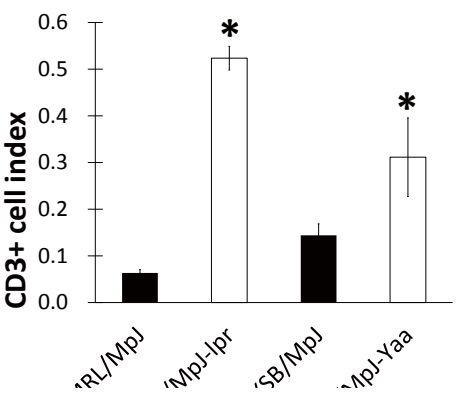
CD3+ cell index
0.6
0.5
0.4
0.3
0.2
0.1
0.0
*
*

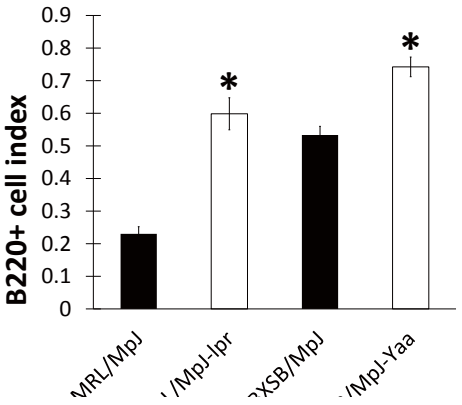
B220+ cell index
0.9
0.8
0.7
0.6
0.5
0.4
0.3
0.2
0.1
0
*
*

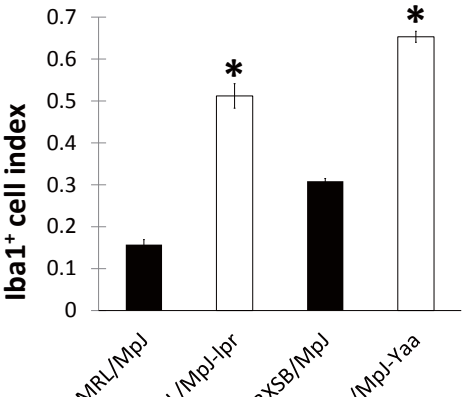
Iba1+ cell index
0.7
0.6
0.5
0.4
0.3
0.2
0.1
0
*
*

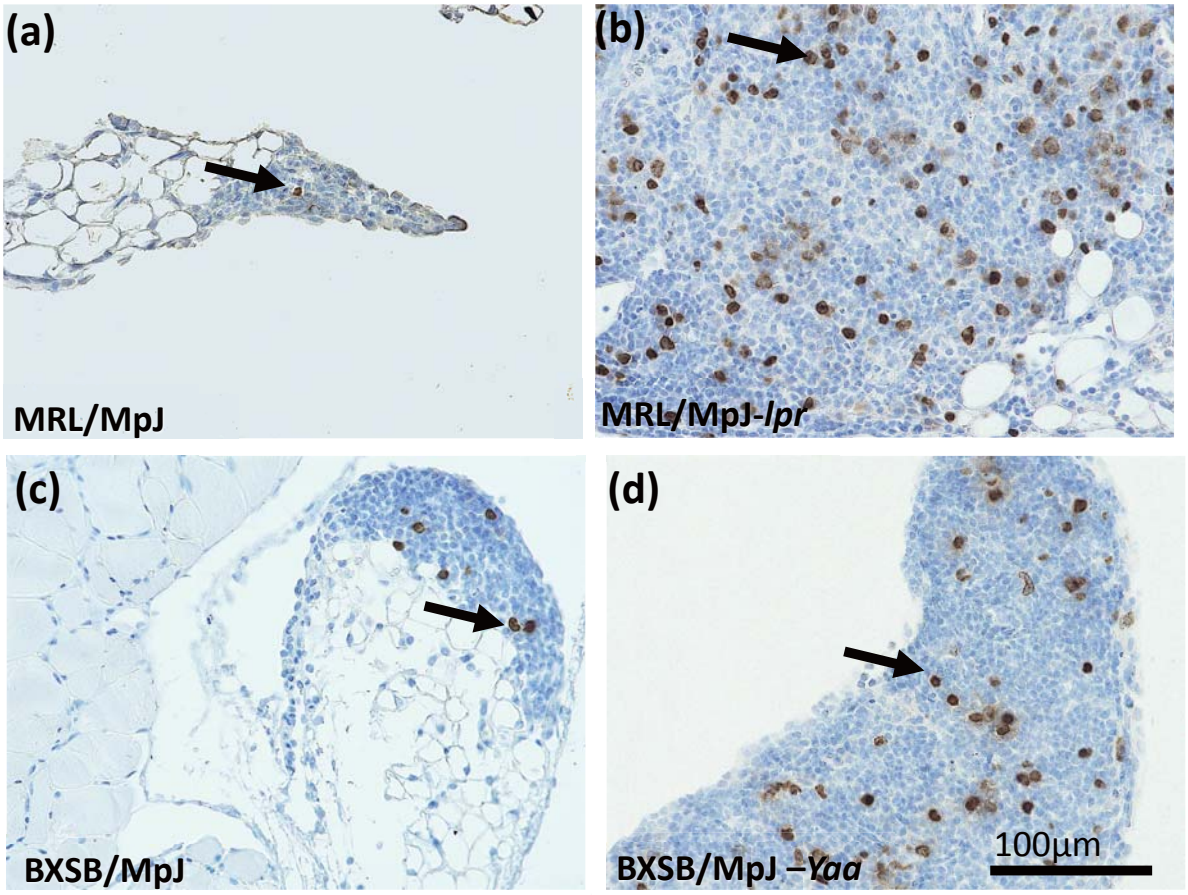

Fig. 4

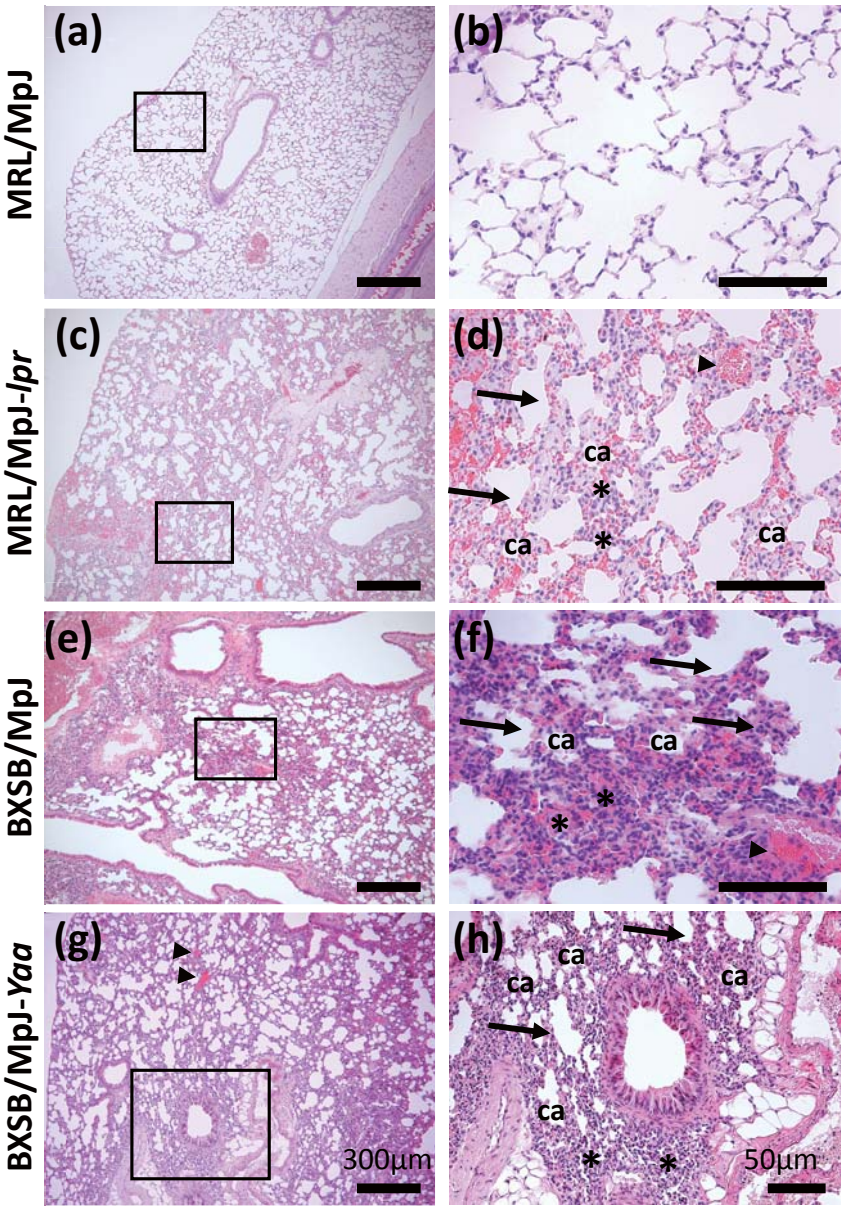
MRL/MpJ
MRL/MpJ-*lpr*
BXSB/MpJ
BXSB/MpJ-*Yaa*
(a)
(b)
(c)
(d)
(e)
(f)
(g)
(h)
ca
300μm
50μm

Fig. 5

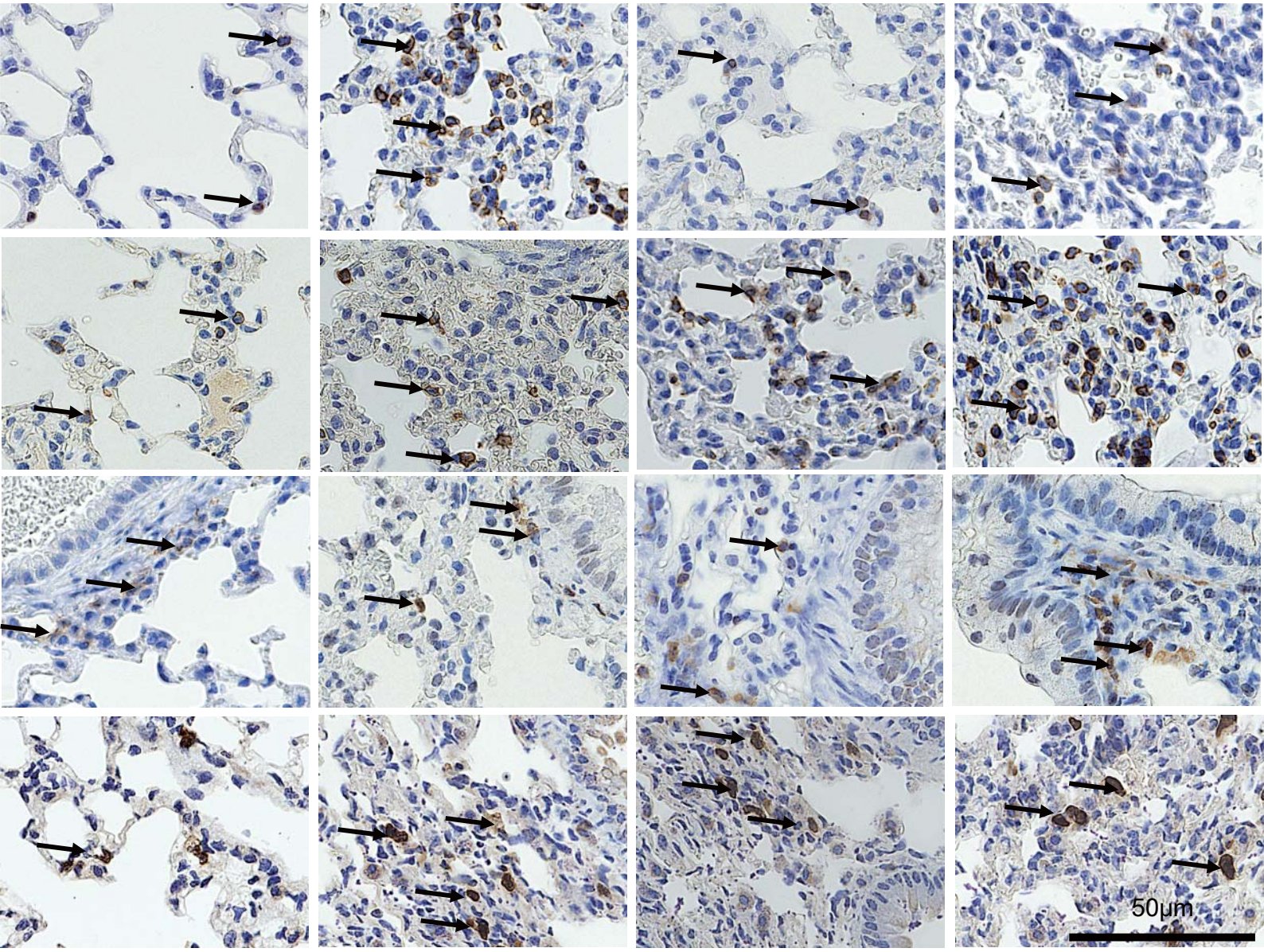
50μm

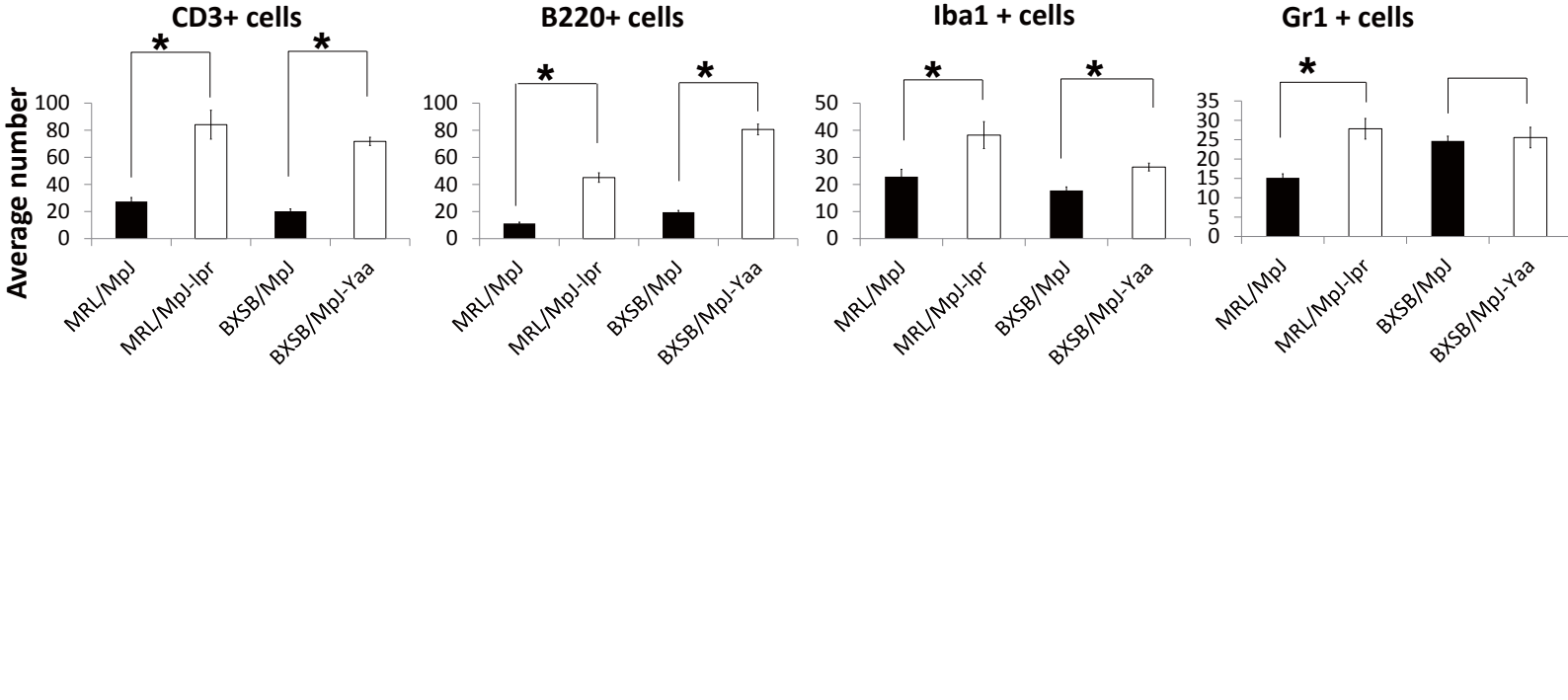
CD3+ cells
B220+ cells
Iba1 + cells
Gr1 + cells
Average number
MRL/MpJ
MRL/MpJ-lpr
BXSB/MpJ
BXSB/MpJ-Yaa